NASA TECHNICAL NOTE

NASA TN D-5196

NASA TN D-5196

EFFECT OF SIZE ON NORMAL-GRAVITY SELF-PRESSURIZATION OF SPHERICAL LIQUID HYDROGEN TANKAGE

by John C. Aydelott and Charles M. Spuckler

Lewis Research Center
Cleveland, Ohio

NATIONAL AERONAUTICS AND SPACE ADMINISTRATION • WASHINGTON, D. C. • MAY 1969

EFFECT OF SIZE ON NORMAL-GRAVITY SELF-PRESSURIZATION OF SPHERICAL LIQUID HYDROGEN TANKAGE

By John C. Aydelott and Charles M. Spuckler

Lewis Research Center
Cleveland, Ohio

NATIONAL AERONAUTICS AND SPACE ADMINISTRATION

For sale by the Clearinghouse for Federal Scientific and Technical Information
Springfield, Virginia 22151 – CFSTI price $3.00

ABSTRACT

A study was conducted at the NASA Lewis Research Center to obtain a correlating parameter which would relate the rate of pressure rise to the volume of spherical liquid-hydrogen tankage. A nonventing 22-inch (56-cm) diameter spherical tank partially filled with liquid hydrogen was subjected to four uniformly heated self-pressurization tests with various combinations of percent filling and heat-transfer rate. These data were compared with data from a similar study on a 9-inch (23-cm) diameter, uniformly heated, spherical tank. The two sets of data verified the analysis which predicted the same change in pressure in each tank for equal values of heat added per unit volume.

EFFECT OF SIZE ON NORMAL-GRAVITY SELF-PRESSURIZATION OF SPHERICAL LIQUID HYDROGEN TANKAGE

by John C. Aydelott and Charles M. Spuckler

Lewis Research Center

SUMMARY

A study was conducted at the NASA Lewis Research Center to obtain a correlating parameter which would relate the rate of pressure rise to the volume of spherical liquid-hydrogen tankage. A nonventing 22-inch (56-cm) diameter spherical tank partially filled with liquid hydrogen was subjected to four uniformly heated, self-pressurization tests with various combinations of percent filling and heat-transfer rate. These data were compared with data from a similar study on a 9-inch (23-cm) diameter, uniformly heated, spherical tank. The two sets of data verified the analysis which predicted the same change in pressure in each tank for equal values of heat added per unit volume.

INTRODUCTION

Hydrogen is very attractive for use as a rocket fuel because of the high specific impulse it produces either when reacted with an oxidizer or when used as a heated expellant as in a nuclear rocket. However, mission planners and tank designers are confronted with problems that result because hydrogen has many properties which set it apart from common fluids. Gaseous hydrogen has a low density, so that it is practical, for space missions, to store hydrogen only as a liquid or solid. The liquid and solid, however, have a very low equilibrium temperature, and this makes it very difficult to insulate a storage container sufficiently to prevent a net heat gain. As heat is continually added to the tank, the tank pressure will rise until venting is required, with an accompanying propellant loss.

The rate of pressure rise in a hydrogen storage tank is highly dependent on the thermal transport properties of hydrogen, which make it possible for subcooled liquid and highly superheated vapor to coexist in the same container. The temperature of the interface between the liquid and vapor phases increases because the interface temperature is

always equal to the saturation temperature corresponding to the increasing total system pressure. The average liquid temperature may increase at a slower rate, thus the liquid bulk becomes subcooled; the average vapor temperature may increase at a faster rate, thus the vapor becomes superheated. The rate of liquid subcooling and vapor superheating will vary with the experimental conditions (tank geometry and percent filling, heat-transfer rate and distribution, etc.) and cause the rate of pressure rise to vary. Consequently, simple thermodynamic analysis often cannot predict the rate of pressure rise in a closed system containing liquid hydrogen, and the possibility of developing scaling parameters should be considered.

The majority of the work in this field has been restricted to cylindrical tanks with heating only on the side walls. Therefore, natural convection theory for vertical plates could be used to predict the heat and mass transfer within the liquid phase. In general, direct heating of the vapor was not considered. An excellent review of this work can be found in reference 1. Of more direct application to understanding the energy transfer processes which take place in any liquid-hydrogen container is the effect of bottom heating (refs. 2 to 5). As the proportion of bottom heating increases, turbulent convection and boiling cause the temperature of the liquid to become more uniform.

In contrast to the available information on cylindrical tanks, very little experimental or theoretical information is available on the normal-gravity self-pressurization of spherical liquid-hydrogen tankage. The earlier work of the first author (ref. 6) determined the importance of the heating configuration on the thermodynamic history of spherical, 9-inch (23-cm) diameter, liquid-hydrogen tankage. Heating the tank only from the top caused pressure rise rates approximately four times greater than those which resulted from heating only the bottom of the tank. Reference 7 presents the results of a self-pressurization test on a 50 000-gallon (189 000-liter) spherical liquid-hydrogen storage tank subjected to a uniform heat-transfer rate of approximately 0.6 Btu per hour per square foot (1.9 W/m^2). The measured rate of pressure rise was approximately 10 times greater than that which would result if the contents of the tank were homogeneous (uniform temperature throughout). The lack of experimental data and the difficulty in analytically relating the rate of pressure rise to the energy input for full-size hydrogen tanks suggest the use of a scaling parameter.

This study was conducted to obtain a correlating parameter for the effect of size on normal-gravity self-pressurization of spherical liquid-hydrogen tankage. This report presents the information obtained from four self-pressurization tests of a spherical 22-inch (56-cm) diameter, liquid-hydrogen tank. The tests were conducted under normal-gravity conditions with approximately uniform heat addition. The effects of the variables, liquid filling (approximately 30 to 80 percent by volume) and average heat-transfer rate (approximately 17 to 64 Btu/(hr)(ft^2) or 53 to 202 W/m^2), on the rate of pressure rise were determined. The data are compared with theoretical analyses and with the results

of reference 6 (9-in. (23-cm) diam tank) to show the effect of size on the self-pressurization of spherical liquid-hydrogen tankage. The information presented in reference 7 (50 000 gal (189 000 liter) tank) is discussed in light of the results of the two smaller tank studies.

ANALYSIS

Thermodynamic Pressure Rise

The first law of thermodynamics is

$$Q = \Delta U + \int P \, dV$$

(Symbols are defined in appendix A.) For a closed, nonexpanding system, all the heat absorbed by the system manifests itself in a change in the total internal energy of the system; that is, for $dV = 0$

$$Q = \Delta U$$

If the system in question is a tank containing a liquid and its vapor, a knowledge of how the added heat affects the internal energy distribution and, thus, the temperature distribution within the tank permits prediction of the total system pressure. This is possible because, for a liquid-vapor system, temperature and pressure are interrelated at the interface (ref. 1).

Since the temperature distribution in the fluid within a cryogenic storage tank is highly complex and is affected by many variables, the most important of which are tank geometry, percent filling, heat-flux rate, and heat-flux distribution, any analytical prediction of pressure rise as a function of heat added must be based on simplifying assumptions. This report makes use of two simple pressure rise models. The mathematical development of each of the models is given in appendix B. The first model assumes homogeneous conditions (uniform temperature) throughout the hydrogen container and is a common calculation that is performed to compare data of this type. The second model assumes that all the energy absorbed by the hydrogen container goes into evaporating liquid and maintaining the vapor at the saturation temperature corresponding to total-system pressure. The liquid-phase temperature remains constant at the saturation temperature corresponding to the initial pressure. These models are not intended to be attempts at describing the process that actually takes place in a nonventing hydrogen con-

tainer, but are intended to be a means of comparing one set of experimental data with another. The position that experimental data assume in relation to the theoretical models on a plot of total pressure against heat added is then a qualitative indication of how the energy is being distributed within the hydrogen container.

Figure 1 is a theoretical plot of tank pressure as a function of heat added for the two energy distribution models. The plot is for a 1-cubic-foot (0.02832-m^3) container and initial liquid fillings of 25, 50, and 75 percent by volume.

Similarity Relation

Starting with the previously presented first law of thermodynamics for a closed non-expanding system

$$Q = \Delta U = \Delta(mu) = \Delta(\rho u)V$$

$$\frac{Q}{V} = \Delta(\rho u)$$

For any fluid the product of density and specific internal energy can be expressed as a function of the pressure and temperature. However, if the fluid is saturated, the pressure and temperature are dependent variables, and the vapor mass fraction of the fluid is also required in order to specify the desired properties

$$\rho u = f(P, T, X)$$

$$\frac{Q}{V} = \frac{\partial f}{\partial P}\Delta P + \frac{\partial f}{\partial T}\Delta T + \frac{\partial f}{\partial X}\Delta X$$

If we wish to compare two systems containing only liquid and gaseous hydrogen, $\partial f/\partial P$, $\partial f/\partial T$, and $\partial f/\partial X$ will be the same for each system. Consideration will be limited to systems of identical geometry, initial percent filling, and heat-transfer rate in order to logically expect similar processes to occur in the two systems. From the last equation, it can be seen that similar changes in pressure, temperature, and vapor mass fraction may then be expected in each tank for equal values of heat added per unit volume. Bailey (ref. 8) reached an identical conclusion.

This similarity relation holds exactly for both of the models presented in the Thermodynamic Pressure Rise section. The reader may approximate the energy input, as determined by these models, that will cause a specified change in pressure for any tank

size or filling. Referring to figure 1, this is done by interpolating to determine the effect of percent filling and by multiplying the heat added by the volume of the tank in cubic feet.

APPARATUS

Liquid Hydrogen Container

Figure 2 is a cross-sectional drawing of the liquid-hydrogen apparatus that consisted of three concentric spheres; the inner sphere contained the liquid hydrogen, the intermediate sphere had electric heating coils mounted on its exterior surface, and the outer sphere served as a vacuum jacket to reduce the gaseous conduction of heat. The outer surface of the inner sphere and the inner surface of the heaters were painted black in order to increase their emissivity. The stainless-steel fill and vent tubes supported the inner sphere.

A heater controller, which basically consisted of a bridge circuit which balanced the resistance of a temperature sensor on each heater with a corresponding rheostat on the control panel, was used to maintain heater temperatures of 360° or 500° R (200 or 278 K).

Instrumentation

Temperature and pressure transducers measured the total system pressure, vacuum-space pressure, surface temperature of the inner sphere, heater, and vacuum jacket, and temperature at 16 locations inside the inner sphere. Figure 3 shows the location of the platinum temperature transducers on the inner sphere and the four carbon resistor temperature rakes that were located within the inner sphere to measure the temperature of the hydrogen liquid and vapor. Figure 4 shows two of the carbon resistor rakes.

At any time prior to a test run, the resistance of any temperature transducer could be determined by the use of a digital ohmeter mounted in the control panel. A very small electric current was passed through a temperature transducer to determine the resistance and thus the temperature of the transducer. When a relatively high current was applied to a carbon resistor, its temperature was quite different depending on whether the temperature probe was in the liquid or vapor phase. This was due to self-heating. Exploitation of this fact, together with careful arrangement of the carbon resistors, made it possible to use the carbon resistors to determine the liquid level in the sphere prior to the start of a test.

A detailed description of the temperature and pressure measuring and recording systems and an analysis of the error associated with them will be found in reference 6.

PROCEDURE

Prior to the assembly of the experiment, thermocouples were attached to the inner sphere, heaters, and vacuum jacket. All temperature transducers were calibrated by submerging the three spheres in a liquid nitrogen bath at 139.5° R (78 K) and by placing the spheres in a carefully controlled temperature chamber at 347°, 486°, 537°, and 601° R (193, 270, 298, and 334 K). After the experiment had been assembled, the inner-sphere temperature transducers were calibrated at 36.4° R (19.1 K) by filling the sphere with liquid hydrogen. Each bridge was calibrated by using a decade box to obtain a voltage versus resistance plot. Prior to each test, the pressure transducers were calibrated with standard pressure gages.

Each of the calibration curves for the temperature transducers and for the bridges was curve fitted using a digital computer. The magnetic data tapes from each test were fed into the digital computer along with the calibration curve fits, and an automatic data reduction program returned printed temperature data at half-second intervals for each transducer. A continuous plot of the output of the pressure transducers was obtained by feeding the output of the magnetic data tapes into a line recorder.

For each of the tests, the experiment was prepared in an identical manner: only the actual test conditions were varied. The space between the inner and outer spheres was evacuated first with a mechanical pump and then with a diffusion pump. Then the inner sphere was filled with liquid hydrogen. The addition of the liquid hydrogen reduced the pressure in the space between the inner and outer spheres due to cryogenic pumping. The capillary tubes (fig. 2) were used to remove liquid from the inner sphere until the approximate desired liquid level was obtained.

For the low heater temperature (low heat-transfer rate) tests, a gas meter installed in the vent line together with the carbon resistors in the inner sphere (described in the Instrumentation section) made it possible to determine the liquid level at the beginning of the test. The resistors accurately determined the liquid position at some time prior to the beginning of the test. At this time the gas meter began to record the volume of hydrogen vapor which then leaves the inner sphere. Measurements of the vapor temperature at the gas meter and the atmospheric pressure determine the density of the vapor. From a knowledge of the volume and density of the vapor, the mass of hydrogen that leaves the inner sphere before the test begins is calculated and the initial percent filling can be determined.

For the high heater temperature (high heat-transfer rate) test, the boiloff rate of the hydrogen was greater than the capacity of the gas meter. Consequently, the eight

carbon resistor temperature transducers that were located near the 50-percent filling level were used to determine the initial filling. By recording the time when the liquid level went below each resistor and extrapolating to the starting time of the test, the initial percent filling could be determined.

The heater controller was set to maintain the desired heater temperature prior to determining the liquid level to eliminate transients. At minus 1 minute, the system began recording data on magnetic tape. At zero time the vent valve was closed and the experiment was allowed to self-pressurize. The tests were terminated either at a nominal pressure of 100 psia (68.95 N/cm^2) or after 45 minutes if the pressure did not reach 100 psia (68.95 N/cm^2). After the experiment reached 100 psia (68.95 N/cm^2) or ran for 45 minutes, the vent valve was opened and the pressure was allowed to decay slowly. If a sufficient amount of liquid hydrogen still remained in the experiment, a similar test at a lower filling was run as soon as the new liquid level had been determined.

EXPERIMENTAL RESULTS

Four quiescent tests with uniform heating were performed. Nominal initial fillings of 30, 50, and 80 percent for the low heat-transfer-rate tests and 50 percent for the high heat-transfer-rate test were desired. Heater temperatures of approximately 360° and 500° R (200 and 278 K) were used for the tests.

Figures 5 to 8, showing pressure and temperature as a function of time, present the data obtained from the test runs. Only enough data symbols are included to identify the curves. Each of the figures is made up of four plots: (a) total pressure as a function of time, (b) outer-sphere and average heater temperature as a function of time, (c) upper inner-sphere internal and surface temperature as a function of time, and (d) lower inner-sphere internal temperature as a function of time. Figures 5 to 7 show the effects of three different percent fillings (31.6, 48.9, and 79.8 percent) for a nearly constant heat-flux, approximately 20 Btu per hour per square foot (63 W/m^2). Figures 6 and 8 show the effects of two different average heat fluxes, 18.9 and 64.4 Btu per hour per square foot (60 and 203 W/m^2), for an approximately half-full sphere.

DISCUSSION OF EXPERIMENTAL RESULTS

External Heat Transfer

A first look at the data might suggest that the rate of pressure rise is the most important parameter to consider when examining a group of tests which had identical heater

temperatures. However, because the hydrogen vapor becomes superheated and because the top of the inner sphere increases in temperature as a test proceeds, this approach can be quite misleading. The heating of the inner sphere increases the temperature of the container wall causing a reduction in the rate of energy input to the hydrogen. This is due to both the reduction in radiant exchange and the energy that is absorbed by the container wall. Higher heater temperatures and lower percent liquid fillings cause increasing inner-sphere temperatures so that the average heat flux to the hydrogen is not a function only of heater temperatures. As a result, it is better to compare the amount of heat that must be added to the hydrogen container to cause a given pressure rise for a particular set of conditions. The method of calculating the net heat addition to the hydrogen container used in these experiments is given in appendix C. The results of this analysis indicate that the main source of energy input to the experiment was radiant exchange from the heaters. Heat transfer due to conduction along the fill and vent tubes and instrumentation wires, as well as gaseous conduction through the vacuum space, was small.

Table I is a summary of the experimental results and the heat-transfer analysis for both the present study and the uniform heating tests of the 9-inch (23-cm) diameter spherical tank (ref. 6). The initial percent filling was determined as explained in the PROCEDURE section. The pressure-rise rate is an average value obtained by dividing the change in the pressure during the test by the total test time. The bulk temperature was assumed to be the lowest recorded temperature from the lower carbon resistor temperature transducers. Dividing the change in the bulk temperature by the change in the saturation temperature during the test gives an indication of how much energy went into heating the liquid and, thus, how nearly homogeneous the liquid is at the end of the test. The maximum change in the vapor temperature is an indication of how much energy went into superheating the vapor. However, the vapor temperature data from the first two tests on the larger spherical tank should not be compared with the other tests. If the first two tests on the larger tank had not been terminated before reaching a pressure of 100 psia (68.95 N/cm^2), the maximum change in the vapor temperature would have been larger. The average heat flux is determined by dividing the total energy input to the hydrogen as calculated in appendix C by the test time and the surface area of the inner sphere. This average is then broken down into the heat flux through the liquid wetted walls and through the walls exposed to vapor by assuming that none of the reradiated heat flux (eq. (C8)) comes from the liquid wetted walls. Breaking the heat flux into parts in this manner clearly shows the effect of the increasing upper inner-sphere temperature which reduces the net radiant heat exchange.

Pressure-Rise Characteristics

Effect of percent filling. - Figure 9 shows the effect of percent filling on the sphere pressure as a function of heat added for six uniformly heated tests. Figure 9(a), taken from reference 6 (9-in. (23-cm) diam spherical tank), and figure 9(b) for the present study (22-in. (56-cm) diam spherical tank), show similar results. The pressurization rate was only slightly affected by varying the percent filling with a trend toward higher pressure-rise rates at higher fillings. In order to understand why the pressure-rise rate is only slightly affected by the percent filling, reference is made to table I. The data for the tests indicate that, as the percent filling is increased, the liquid becomes more subcooled (less homogeneous) and the vapor becomes less superheated (more homogeneous). These two effects tend to counterbalance each other.

Effect of heat-transfer rate. - Figure 10 shows the effect of heat-transfer rate on sphere pressure as a function of total heat added for the approximately 50-percent filled, uniformly heated, quiescent tests. Figure 10(a), taken from reference 6, and figure 10(b), for the present study, show similar results. Since the two coordinates, pressure

TABLE I. - SUMMARY OF EXPERIMENTAL RESULTS AND HEAT-TRANSFER ANALYSIS[a]

Test	Initial filling, percent	Average pressure-rise rate		Liquid-temperature ratio, $\Delta T_b/\Delta T_{sat}$	Maximum vapor temperature change		Unit area heat-transfer rate q/A_1					
							Average		Wetted area		Dry area	
		psi/min	N/cm^2/min		°R	K	Btu/(hr)(ft^2)	W/m^2	Btu/(hr)(ft^2)	W/m^2	Btu/(hr)(ft^2)	W/m^2
22-in. (56-cm) diameter spherical tank-uniform heating												
1	31.6	1.23	0.85	0.59	[b](130)	[b](72)	16.9	53	22.3	70	13.6	43
2	48.9	1.41	.97	.48	[b](155)	[b](86)	18.9	60	22.0	69	15.8	50
3	79.8	2.04	1.4	.34	164	91	21.9	69	22.6	71	20.2	64
4	54.2	4.78	3.3	.51	222	123	64.4	203	83.7	264	41.6	131
9-in. (23-cm) diameter spherical tank-uniform heating (ref. 6)												
1	34.6	3.5	2.4	0.55	110	61	17.5	55	20.0	63	15.7	49
2	51.4	3.6	2.5	.46	115	64	18.2	57	20.0	63	16.4	52
3	34.9	11.3	7.8	.62	212	118	59.9	189	80.3	253	45.8	144
4	48.9	13.5	9.3	.47	200	111	65.0	205	80.7	254	48.9	154
5	76.5	17.0	11.7	.32	159	88	72.6	229	80.5	254	54.1	171
6	36.8	19.3	13.3	.61	258	143	105.4	332	148.0	466	74.5	235
7	50.7	23.6	16.3	.47	245	136	111.6	352	142.7	450	78.4	247
8	77.2	30.3	20.9	.31	182	101	128.6	405	141.9	447	97.7	308

[a]Quantities defined in heat transfer analysis and test results section.

[b]Test terminated before reaching 100 psia (68.95 N/cm^2).

and heat added, are the integrals over time of pressure-rise rate and heat-transfer rate, coincident test data indicate a linear relation between pressure-rise rate and heat-transfer rate; that is doubling the heat-transfer rate will double the pressure-rise rate. This linear relation was followed almost exactly for all the approximately 50-percent filled, uniformly heated, quiescent tests.

Internal Heat and Mass Transfer

Liquid bulk. - Analysis based on the modified Rayleigh number ($Ra = C_p g\beta\rho^2 qD^4/k^2\mu A$) for the present study and the work of reference 6 ($Ra \approx 10^{10}$ to 10^{13}), indicates that the mode of heat transfer in the liquid bulk would be turbulent convection (refs. 9 to 11). However, a summary of liquid-hydrogen boiling studies presented in references 12 and 13 indicate that, at the heat fluxes employed for these tests, nucleate boiling is quite likely to occur. An essentially uniform-temperature liquid bulk would be anticipated for either turbulent convection or boiling heat transfer. Because a uniform-temperature liquid bulk was experimentally observed, it is probable that, at the lower heat fluxes, the heat and mass transfer in the liquid was dominated by turbulent convection with some boiling entering in at the higher heat fluxes.

In contrast to the results obtained with the smaller tanks, is the data (ref. 7) obtained from a much larger spherical tank (50 000 gal (189 000 liter)). For this test the heat-transfer rate was approximately 0.6 Btu per hour per square foot (1.9 W/m^2). The pressure-rise rate was approximately 10 times greater than the calculation based on homogeneous conditions, which is much greater than for any of the small tank tests. It is believed that, due to the low heat-transfer rate, a laminar natural convection boundary layer along the tank wall carried the incoming energy directly to the liquid surface. This conclusion is based on the fact that very little heating of the liquid bulk was observed during the experiment. Natural convection boundary-layer flow would be expected if the Rayleigh number for this test was less than the Rayleigh number for the small tank tests. However, the Rayleigh number, based on tank diameter, for the reference 7 test is much larger due to the fourth power dependence of the Rayleigh number on the significant dimension. Consequently, either this type of Rayleigh number analysis is not valid or the characteristic dimension in the Rayleigh number should be some other quantity such as the boundary-layer thickness.

Vapor. - The heat-transfer processes which take place in the vapor are not clearly understood. The fact that the lines of constant temperature in the vapor were horizontal, with increasing temperature at higher vertical positions, may rule out the possibility of any convective flow. The validity of this point is shown by figure 11, which is a typical plot of inner-sphere temperature as a function of vertical position. The liquid-vapor in-

terface is located at a height to radius ratio of approximately 1. This figure shows that for any given time, the temperature of the vapor space was only a function of the vertical coordinate, since the data for all the instrumentation, both centrally located and near the container wall, had the same temperature profile. It is possible that an involved conduction analysis could predict the vapor temperature gradients; however, the results of the study presented in reference 14 indicate that the increasing system pressure could cause fluid motion which would dominate any conduction effects.

Liquid-vapor interface. - The transfer of heat and mass across the liquid-vapor interface, either by evaporation or condensation, is also a process that is not well understood. Reference 15 presents an analysis based on irreversible thermodynamics that will predict the behavior of a fluid as it changes phase. However, the three transport coefficients that are necessary for solution of the equations must be experimentally determined. To the authors knowledge, the values of these coefficients for hydrogen are not available.

Liquid-thermal layer. - The liquid-thermal layer is the variable temperature region in the liquid between the liquid-vapor interface and the uniform temperature liquid bulk. Since the liquid bulk was always experimentally observed to be subcooled and the liquid-vapor interface is always saturated, it is reasonable to assume that conduction heat-transfer could account for the temperature gradients that exist in the liquid thermal layer. Here analysis is difficult because of the wide diversity of available data for the thermal conductivity of liquid hydrogen (ref. 16).

Effect of Tank Size

As can be seen, a great deal more basic research is necessary before the internal heat and mass-transfer processes which take place in a closed cryogenic container can be predicted analytically. Until this information is available, the rate of pressure rise in a closed cryogenic container must be determined experimentally. However, the use of models is a common engineering tool that can be used once scaling laws have been derived. The ANALYSIS section shows that the same pressure rise should result in two tanks of similar geometry, percent filling, and heating configuration if the ratio of the total heat added to tank volume is the same. The effect of large differences in heat-transfer rate was shown by the comparison of the results of reference 7 (50 000-gal (189 000-liter) spherical tank) with the results obtained in the smaller tanks. The large tank had a rate of pressure rise approximately 10 times greater than would result from the homogeneous analysis while the rate of pressure rise in the smaller tanks was three to four times greater than homogeneous. It is believed that this difference in comparative pressure-rise rates is due to the large difference in heat-transfer rates between the

larger and small tanks. Consequently, for scaling purposes, the heat-transfer rates must be such that similar heat- and mass-transfer processes take place in the liquid bulk. Figure 12 is a plot of pressure as a function of total heat added divided by tank volume for two pairs of similar tests performed using the two smaller spherical liquid-hydrogen tanks. These two pairs of data were chosen because their initial fillings were nearly identical, thus fulfilling one of the restrictions postulated in the ANALYSIS section. These data fell within a narrow band. However, as shown in figure 9, the effect of percent filling was small, so that all the data would fall within a narrow band, thus supporting the analysis which predicted that the effect of size on the self-pressurization of hydrogen tankage can be expressed as a simple geometric relation.

Energy Distribution

In order to better understand the experimental results, an analysis was performed to determine what percentage of the incoming energy resulted in heating of the liquid bulk, the liquid-thermal layer, evaporation of liquid, and superheating of the vapor. The details of these energy-distribution calculations will be found in appendix D. Table II is a summary of the results of the energy distribution analysis for both the present study

TABLE II. - RESULTS OF ENERGY-DISTRIBUTION ANALYSIS

Test	Average filling, percent	Energy input to liquid wetted walls, percent of total	Liquid			Vapor	Evaporation
			Total	Bulk	Thermal layer		
			Heat added, percent of total energy input				
22-in. (56-cm) diameter spherical tank-uniform heating							
1	32.6	50.0	75.8	45.4	30.4	15.0	9.2
2	50.1	58.3	81.9	64.7	17.2	11.4	6.7
3	81.5	74.2	93.9	82.7	11.2	4.8	1.3
4	56.0	70.5	82.9	67.6	15.3	14.0	3.1
9-in. (23-cm) diameter spherical tank-uniform heating (ref. 6)							
1	35.8	46.4	77.4	32.5	44.9	8.8	13.8
2	52.9	57.2	83.0	51.7	31.3	6.7	10.3
3	36.7	54.9	76.1	39.1	37.0	18.1	5.8
4	50.4	62.7	79.4	58.4	21.0	15.4	5.2
5	78.2	77.5	91.1	64.6	26.5	7.7	1.2
6	38.4	59.2	74.4	47.8	26.6	22.0	3.6
7	52.2	66.0	77.4	65.5	11.9	18.7	3.9
8	78.7	77.1	90.7	63.8	26.9	8.7	.6

and the uniform-heating tests of reference 6. The analysis shows that the energy input to the dry walls heated the vapor, supplied the necessary energy for evaporation, and heated some of the liquid since the energy input to the liquid wetted walls was always less than the input to the liquid. The energy input to the liquid wetted walls heated the liquid bulk, and in some cases, a portion of the liquid-thermal layer. Essentially, the same conclusion was reached by the authors of reference 17 as a result of their tests on a 625-gallon (2360-liter) cylindrical hydrogen Dewar.

The pressure-rise rate in the hydrogen container for the uniformly heated tests is primarily a function of the energy input to the dry walls since the energy input to the liquid wetted walls only heats the liquid. The only contribution that the heating of the liquid wetted walls makes to the container pressure is due to the thermal expansion of the liquid. Liquid hydrogen does have a relatively high coefficient of thermal expansion, but this effect is secondary to the energy input to the vapor and for evaporation in determining the rate of pressure rise.

The minor differences in the energy input distribution explain the slight deviations in the results that were obtained from the two small hydrogen tanks (fig. 12). As the heat-transfer rate was increased, the contents of the 9-inch (23-cm) tank became slightly less homogeneous (fig. 10(a)); while the contents of the 22-inch (56-cm) tank remained essentially the same (fig. 10(b)). This difference is attributed to the thicker wall of the 22-inch (56-cm) tank, which absorbed a larger proportion of the incoming energy at the highest heat-transfer rates and caused less heating of the vapor (see tables I and II).

SUMMARY OF RESULTS

A nonventing 22-inch (56-cm) diameter spherical tank partially filled with liquid hydrogen was subjected to four uniformly heated self-pressurization tests. These tests were conducted with various combinations of liquid filling (approximately 30 to 80 percent by volume) and heat-transfer rate (approximately 17 to 64 Btu/(hr)(ft^2) or 53 to 202 W/m^2). These data were compared with data from a similar study performed on a 9-inch (23-cm) diameter, uniformly heated, spherical tank (ref. 6) and with the self-pressurization of a 50 000-gallon (189 000-liter) spherical liquid-hydrogen storage tank (ref. 7). For the range of variables investigated, the following results were obtained:

1. The data from the 9-inch (23-cm) and 22-inch (56-cm) diameter spherical tank tests verified the analysis that predicted that the effect of size on self-pressurization of hydrogen tankage can be expressed as a simple geometric relation involving the heat added per unit volume. This conclusion is supported by the fact that the pressure data, plotted as a function of heat added per unit volume, fell within a narrow band.

2. The pressure-rise rate increased almost linearly with increasing heat-transfer rate; however, as the heat-transfer rate was increased, the contents of the 9-inch (23-cm) tank became slightly less homogeneous while the contents of the 22-inch (56-cm) tank remained essentially the same. This difference is attributed to the thicker wall of the 22-inch (56-cm) tank which absorbed a larger proportion of the incoming energy at the higher heat-transfer rates and caused a change to more bottom heating.

3. For both the 9-inch (23-cm) and 22-inch (56-cm) tanks the pressure rise rate was only slightly affected by varying the percent filling with a trend toward increasing pressure-rise rates at higher fillings.

4. The 50 000-gallon (189 000-liter) spherical liquid-hydrogen storage tank (ref. 7) had a much greater rate of pressure rise, when compared with the homogeneous analysis, than either of the smaller tanks. This difference was attributed to a different mode of heat transfer in the liquid. At the low heat fluxes encountered in the reference 7 experiment (0.6 Btu/(hr)(ft^2) or 1.9 W/m^2), heat is transported in the liquid by laminar natural convection rather than turbulent convection as is the case for the tests on the smaller tanks so that larger temperature gradients and nonhomogeneous conditions result.

Lewis Research Center,
National Aeronautics and Space Administration,
Cleveland, Ohio December 12, 1968,
124-09-17-01-22.

APPENDIX A

SYMBOLS

A	surface area, ft^2; m^2
a	accommodation coefficient
B_{jl}	absorption factor
C_p	specific heat, Btu/(lb)(^oR); J/(kg)(K)
C_V	specific heat, Btu/(lb)(^oR); J/(kg)(K)
D	diameter, ft; m
F	angle factor
g	acceleration due to gravity, ft/sec^2; m/sec^2
k	thermal conductivity, Btu/(hr)(ft)(^oR); W/(m)(K)
L	length, ft; m
M	molecular weight
m	mass, lb; kg
P	pressure, psia; N/cm^2
pf	filling by volume, percent
Q	heat added, Btu; J
q	heat-transfer rate, Btu/hr; W
R	universal gas constant, 1.986 Btu/(lb)(mole)(^oR); 8.3143 J/(mole)(K)
r	reflectivity
T	absolute temperature, ^oR; K
t	time, hr
U	total internal energy, Btu; J
u	specific internal energy, Btu/lb; J/kg
V	volume, ft^3; m^3
X	vapor mass fraction
x	linear distance, ft; m
β	coefficient of thermal expansion, $1/^oR$; 1/K
γ	ratio of specific heats, C_p/C_v
ϵ	emissivity
μ	dynamic viscosity, (lb)(sec)/ft^2; (N)(sec)/m^2
ρ	density, lb/ft^3; kg/m^3
σ	Stefan-Boltzmann constant, 0.1713×10^{-8} Btu/(hr)(ft^2)($^oR^4$); 5.6697×10^{-8} W/(m^2)(K^4)

Subscripts:

a	absorbed
av	average
b	liquid bulk
ev	evaporation
f	final or any intermediate state
gc	gaseous conduction
i	initial state
j	summation variable
L	at x = L
ℓ	liquid
l	liquid thermal layer

m	mean or average value	v	vapor
max	maximum	vg	at vacuum gage
n	summation variable	w	wall
r	radiant	0	at $x = 0$
rr	reradiated	1	inner sphere
s	system	2	upper heater
sat	saturation	3	lower heater
sc	solid conduction	4	opening in upper heater
st	stored	5	combined upper and lower heaters

APPENDIX B

THERMODYNAMIC ANALYSIS

One method of analyzing a system thermodynamically is to define the conditions at the beginning and the end of a process; then the necessary input to the system can be determined. For the problem of a liquid-hydrogen storage tank, which is sealed at the beginning of the test, the initial condition is that the tank contains a homogeneous mixture at atmospheric pressure with a known percent filling by volume. The final condition is defined by the model being considered. For a nonexpanding closed system, the input is heat, and, as stated by the first law of thermodynamics

$$Q = \Delta U \tag{B1}$$

Equation (B1) may be written in the form

$$Q = U_f - U_i = (m_{\ell,f}u_{\ell,f} + m_{v,f}u_{v,f}) - (m_{\ell,i}u_{\ell,i} + m_{v,i}u_{v,i}) \tag{B2}$$

The density and specific internal energy of each phase at state i can be found if the system is known to be homogeneous and at the saturation temperature corresponding to atmospheric pressure (ref. 18). The total internal energy at state i can then be determined because

$$m_{\ell,i} = \rho_{\ell,i}\frac{(pf)_i}{100}V \tag{B3}$$

$$m_{v,i} = \rho_{v,i}\left[1 - \frac{(pf)_i}{100}\right]V \tag{B4}$$

For a closed nonexpanding system, the mass of the liquid plus the mass of the vapor is a constant; consequently, the system density is a constant

$$\rho_s = \frac{(pf)_i}{100}\rho_{\ell,i} + \left[1 - \frac{(pf)_i}{100}\right]\rho_{v,i} \tag{B5}$$

Homogeneous model. - State f (and thus the density and internal energy of each

phase) is defined by the fact that the system is homogeneous and is at the saturation temperature corresponding to the system pressure. Equation (B5), written for state f, can be solved for the percent filling at state f

$$(pf)_f = \left(\frac{\rho_s - \rho_{v,f}}{\rho_{\ell,f} - \rho_{v,f}}\right) 100 \tag{B6}$$

The total internal energy at state f can then be determined using equation (B6)

$$m_{\ell,f} = \rho_{\ell,f} \frac{(pf)_f}{100} V \tag{B7}$$

and

$$m_{v,f} = \rho_{v,f} \left[1 - \frac{(pf)_f}{100}\right] V \tag{B8}$$

The amount of heat required to reach state f for the homogeneous model can now be calculated by using equations (B2) to (B4) and (B7) and (B8).

Surface-evaporation model. - State i is the same as that for the previous model so that the total internal energy at state i is found by the identical procedure. The surface-evaporation model is based on the concept that all the energy goes into evaporating the liquid and maintaining the vapor at the saturation temperature. If it is assumed that the liquid is incompressible, then the density and internal energy of the remaining liquid will be unaltered by the process; that is, $\rho_{\ell,i} = \rho_{\ell,f}$ and $u_{\ell,i} = u_{\ell,f}$. The density and internal energy of the vapor are defined by the fact that the vapor is homogeneous and at the saturation temperature corresponding to the final system pressure. Equation (B5), written for state f, can be solved for the percent filling at state f:

$$(pf)_f = \left(\frac{\rho_s - \rho_{v,f}}{\rho_{\ell,i} - \rho_{v,f}}\right) 100 \tag{B9}$$

The mass of liquid and vapor at state f can then be determined using equation (B9)

$$m_{\ell,f} = \rho_{\ell,i} \frac{(pf)_f}{100} V \tag{B10}$$

and

$$m_{v,f} = \rho_{v,f} \left[1 - \frac{(pf)_f}{100}\right] V \tag{B11}$$

The total internal energy at state f can now be determined, and from equations (B2) to (B4) and (B10) and (B11) the heat required to reach state f for the surface-evaporation model can be calculated.

APPENDIX C

HEAT-TRANSFER ANALYSIS

The amount of energy absorbed by the contained hydrogen is equal to the heat transferred to the sphere by radiation, solid conduction, and gaseous conduction minus the amount of energy stored in the container itself; that is,

$$Q_a = (q_r + q_{sc} + q_{gc})\Delta t - Q_{st} \tag{C1}$$

The amount of heat transferred by thermal radiation from the heated intermediate sphere to the inner sphere is determined by the method presented in reference 19. For the radiant exchange calculations the outside of the inner sphere is assigned the number 1, the inside of the upper heater, number 2, the inside of the lower heater, number 3, and the opening in the upper heater, number 4. The net rate of radiant heat absorbed by the inner sphere when both heaters are installed is

$$q_1 = \sum_{j=1}^{4} \sigma B_{j1} \epsilon_j A_j T_j^4 - \sigma \epsilon_1 A_1 T_1^4 \tag{C2}$$

where B_{j1}, the absorption factor, is defined as the fraction of the total radiant-energy emission of surface j which is absorbed by surface 1. The absorption factors are determined by solution of the following simultaneous equations:

$$(F_{11}r_1 - 1)B_{11} + F_{12}r_2B_{21} + F_{13}r_3B_{31} + F_{14}r_4B_{41} + F_{11}\epsilon_1 = 0 \tag{C3}$$

$$F_{21}r_1B_{11} + (F_{22}r_2 - 1)B_{21} + F_{23}r_3B_{31} + F_{24}r_4B_{41} + F_{21}\epsilon_1 = 0 \tag{C4}$$

$$F_{31}r_1B_{11} + F_{32}r_2B_{21} + (F_{33}r_3 - 1)B_{31} + F_{34}r_4B_{41} + F_{31}\epsilon_1 = 0 \tag{C5}$$

$$F_{41}r_1B_{11} + F_{42}r_2B_{21} + F_{43}4_3B_{31} + (F_{44}r_4 - 1)B_{41} + F_{41}\epsilon_1 = 0 \tag{C6}$$

This technique treats all diffuse-radiation circumstances and requires only a knowledge of the geometry of the four surfaces, the average temperature of the surfaces, and the emissivity of the surfaces. Lewis Research Center personnel experimentally obtained the emissivity of the inner surface of the heaters and the outer surface of the hydrogen

container (fig. 13) by using a sample identical to both surfaces. Because of the wires and tubes coming through the hole in the upper heater, the heat radiated through the hole from the outer sphere was assumed to be emitted from a black body.

Because of the variation in temperature of the inner sphere, the last term in equation (C2) was expressed as an integral and called the inner-sphere reradiated heat flux

$$q_{1,rr} = \int_{A_1} \sigma \epsilon T^4 dA \tag{C7}$$

where A_1 is the surface area of the inner sphere. This integral was approximated by the summation

$$q_{1,rr} \approx \sum_{j=1}^{n} \sigma \epsilon_j T_j^4 \Delta A_j \tag{C8}$$

It was assumed that the hydrogen temperature profiles were symmetric with respect to the vertical axis. In other words, at any time during a test all vertical planes passing through the center of the inner sphere would exhibit identical temperature patterns, and the left side of such a plane would be the mirror image of the right side. This assumption is based on the fact that the sphere, heaters, fill and vent tubes, instrumentation wires, and liquid-vapor interface all have symmetry with respect to the vertical axis; consequently, there is no reason to anticipate that the hydrogen temperature profiles would be different on opposite sides of the container. Based on this assumption, horizontal uniform temperature sections could be used to divide the sphere into elemental surface areas. A digital computer was used to curve fit the emissivity as a function of temperature curve and the inner-sphere temperature as a function of position for each time interval. An average temperature for each elemental area was used to determine the local emissivity, and the summation was performed every 30 seconds by using a digital computer.

The energy stored in the container at any time interval was also expressed as an integral

$$Q_{st} = \int_{V_{1,w}} \rho C_p T dV \tag{C9}$$

where $V_{1,w}$ is the volume of the container wall. This integral was approximated by the summation

$$Q_{st} \approx \sum_{j=1}^{n} \rho C_{p,j} T_j \Delta V_j \tag{C10}$$

Assuming the same temperature distribution, a digital computer was used to curve fit the stainless-steel specific heat as a function of temperature curve found in figure 14 (ref. 20) and the inner-sphere temperature as a function of position curves for each time interval. An average temperature for each elemental volume was used to determine the specific heat and the summation was performed every 30 seconds by using a digital computer.

The differential equation and boundary conditions for one-dimensional heat transfer by solid conduction are the following:

$$\frac{d}{dx}\left(k \frac{dT}{dx}\right) = 0 \begin{cases} \text{at } x = 0, \ T = T_0 \\ \\ \text{at } x = L, \ T = T_L \end{cases} \tag{C11}$$

At the very low temperatures encountered with the use of liquid hydrogen, the thermal conductivity of most materials is highly temperature dependent and can be expressed as some function of the absolute temperature. Substituting the boundary conditions in equation (C11) and integrating (ref. 19) result in

$$\frac{q_{sc}}{A} = k_m \frac{T_0 - T_L}{L} \tag{C12}$$

where

$$k_m = \frac{1}{T_L - T_0} \int_{T_0}^{T_L} k(T) dT \tag{C13}$$

Figure 15 shows the stainless-steel thermal conductivity as a function of temperature (ref. 20) and the curve fit which was used to perform the necessary integration in equation (C13). The amount of heat transferred through the vacuum space by gaseous conduction was determined by the following equation (ref. 20).

$$\frac{q_{gc}}{A_1} = \frac{1}{2}\left[\frac{a_1 a_5}{a_5 + a_1(1 - a_5)A_1/A_5}\right]\left(\frac{\gamma + 1}{\gamma - 1}\right)\sqrt{\frac{R}{2\pi}}\frac{P}{\sqrt{T_{Vg}M}}(T_5 - T_1) \qquad \text{(C14)}$$

APPENDIX D

ENERGY DISTRIBUTION ANALYSIS

The total volume of the hydrogen container as it appears in this analysis included the volume of the plumbing up to the seal-off point of the experiment. Expansion of the container due to the increasing pressure was neglected.

The total test time was divided into 30-second intervals, and by using an iterative method the following calculations were performed for each time interval. As a first approximation, it was assumed that the liquid level did not change between successive time intervals so that the volume of vapor could be determined.

Referring to figure 11, the energy distribution analysis was based on the assumption that the vapor space could be divided into horizontal uniform temperature disks. Each disk or elemental volume approximated a region of constant temperature and pressure. Since two thermodynamic properties are known, for each elemental volume, any other property can be determined. The properties of particular interest are the density and specific internal energy. The equations that were used to generate the hydrogen tables (ref. 18) were curved fitted using a digital computer so that the desired properties were readily available once the temperature and pressure were obtained from the experimental data. By using the elemental volumes to perform a summation (approximating an integration) it is possible to determine the total mass and internal energy of the vapor space at any time.

$$m_v = \int_{V_v} dm_v \tag{D1}$$

$$U_v = \int_{V_v} u_v \, dm_v \tag{D2}$$

These two integrals were approximated by the summations

$$m_v \approx \sum_{j=1}^{n} \rho_{v,j} \, \Delta V_{v,j} \tag{D3}$$

$$U_v \approx \sum_{j=1}^{n} u_{v,j} \rho_{v,j} \Delta V_{v,j} \tag{D4}$$

At any time these summations can be evaluated by using a digital computer. It is first necessary to curve fit the vapor temperature against position data for the test times of interest. The computer can then determine the necessary properties, from the hydrogen property curve fits, for each elemental volume and perform the necessary mathematical operations. The energy input to the vapor during any time interval is

$$Q_v = U_{v,f} - U_{v,i}$$

The change in the mass of the vapor is

$$\Delta m_v = m_{v,f} - m_{v,i} \tag{D5}$$

The energy input that results in evaporation is

$$Q_{ev} = (\Delta m_v)(\text{Heat of vaporization}) \tag{D6}$$

The energy input to the liquid is determined by subtracting the energy input to the vapor and the energy input that results in evaporation from the total energy input to the contained hydrogen.

$$Q_\ell = Q_a - Q_v - Q_{ev} \tag{D7}$$

To explore further the energy distribution within the liquid phase, the energy input to the liquid was broken down into two parts: the energy that went into the bulk of the liquid and the energy that went into heating the thermal layer between the saturated liquid-vapor interface and the bulk of the liquid. Figure 11 shows that the bulk temperature, or lowest recorded temperature, is representative of a large portion of the liquid mass. For the purpose of mathematical computation, a linear temperature gradient from the bulk temperature to the saturation temperature at the interface was assumed. It is realized that for some of the tests this is a poor approximation to the actual temperature gradient, but the analysis based on this assumption helps to explain further how energy is transported and distributed within the liquid hydrogen. The bulk temperature, at any time is determined from the instrumentation and the thermal layer average temperature is

$$T_{\ell} = \frac{T_b + T_{sat}}{2} \tag{D8}$$

Since the liquid-vapor interface is always at the saturation temperature, the average internal energy of the liquid initially corresponds to the saturated temperature and pressure and at any later time is

$$u_{\ell,av} = u_{\ell,i} + \frac{Q_{\ell}}{m_{\ell}} \tag{D9}$$

where

$$m_{\ell} = m_{\ell,i} - \Delta m_v$$

At any time the energy stored in the liquid must be equal to the sum of the energy stored in the two regions such that,

$$m_{\ell} u_{\ell,av} = m_b u_b + m_{\ell} \frac{u_b + u_{sat}}{2} \tag{D10}$$

The total mass of liquid is equal to the sum of the mass of liquid in the two regions.

$$m_{\ell} = m_b + m_{\ell} \tag{D11}$$

Combination of equations (D10) and (D11) yields

$$m_b = m_{\ell} \frac{(u_{\ell,sat} + u_b - 2u_{\ell,av})}{u_{\ell,sat} - u_b} \tag{D12}$$

All the liquid is initially saturated so the energy input to the bulk is

$$Q_b = m_{b,f} u_{b,f} - m_{\ell,i} u_{\ell,sat,i} \tag{D13}$$

Subtracting the energy input to the bulk from the total energy input to the liquid yields

$$Q_{\ell} = Q_{\ell} - Q_b \tag{D14}$$

To determine the validity of the initial assumption, the percent filling of the inner sphere was recomputed

$$pf = \frac{m_\ell}{\rho_{\ell,av} V} \times 100 \tag{D15}$$

where $\rho_{\ell,av}$ is determined by using the computer and the values of the total sphere pressure and $u_{\ell,av}$ as input. This new value of percent filling allows the vapor volume to be recomputed and the calculations are performed again starting with equation (D1). This cycle is repeated until the liquid mass changes by less than 0.1 percent; the computer then proceeds to the next time interval.

REFERENCES

1. Clark, J. A.: A Review of Pressurization, Stratification, and Interfacial Phenomena. International Advances in Cryogenic Engineering. Vol. 10. K. D. Timmerhaus, ed., Plenum Press, 1965, pp. 259-283.

2. Scott, L. E.; Robbins, R. F.; Mann, D. B.; and Birmingham, B. W.: Temperature Stratification in a Nonventing Liquid Helium Dewar. J. Nat. Bureau Standards, vol. 64C, no. 1, Jan.-Mar. 1960, pp. 19-23.

3. Tatom, J. W.; Brown, W. H.; Knight, L. H.; and Coxe, E. F.: Analysis of Thermal Stratification of Liquid Hydrogen in Rocket Propellant Tanks. Advances in Cryogenic Engineering. Vol. 9. K. D. Timmerhaus, ed., Plenum Press, 1964, pp. 265-272.

4. Anderson, Bernhard H.; and Kolar, Michael J.: Experimental Investigation of the Behavior of a Confined Fluid Subjected to Nonuniform Source and Wall Heating. NASA TN D-2079, 1963.

5. Vliet, G. C.; and Brogan, J. J.: Experimental Investigation of the Effects of Baffles on Natural Convection Flow and on Stratification. Proceedings of the Conference on Propellant Tank Pressurization and Stratification. Vol. 2. NASA TM X-57140, 1965, pp. 61-86.

6. Aydelott, John C.: Normal Gravity Self-Pressurization of 9-Inch (23-cm) Diameter Spherical Liquid Hydrogen Tankage. NASA TN D-4171, 1967.

7. Liebenberg, D. H.; and Edeskuty, F. J.: Pressurization Analysis of a Large-Scale Liquid-Hydrogen Dewar. International Advances in Cryogenic Engineering. Vol. 10. K. D. Timmerhaus, ed., Plenum Press, 1965, pp. 284-289.

8. Bailey, T.; Convington, D.; Fearn, R.; Pedreyra, D.; Perchoduk, T.; Richards, H.; and Merrill, H.: Analytical and Experimental Determination of Liquid Hydrogen Temperature Stratification. Rep. CR-63-5, Martin Co. (NASA CR-56979), Apr. 1963.

9. Dropkin, D. and Somerscales, E.: Heat Transfer by Natural Convection in Liquids Confined by Two Parallel Plates Which are Inclined at Various Angles with Respect to the Horizontal. J. Heat Transfer, vol. 87, no. 1, Feb. 1965, pp. 77-84.

10. Schwartz, S. H.; and Holmes, L. A.: Flow Visualization and Thermal Stratification of Water in a Horizontal Cylinder and a Sphere. Proceedings of the Conference on Long-Term Cryo-Propellant Storage in Space. NASA TM X-60666, 1966, pp. 163-172.

11. Lock, G. S. H.; Gort, C.; and Pond, G. R.: A Study of Instability in Free Convection From an Inclined Plate. Appl. Sci. Res., vol. 18, no. 3, Nov. 1967, pp. 171-182.

12. Drayer, D. E.; and Timmerhaus, K. D.: An Experimental Investigation of the Individual Boiling and Condensing Heat-Transfer Coefficients for Hydrogen. Advances in Cryogenic Engineering. Vol. 7. K. D. Timmerhaus, ed., Plenum Press, 1962, pp. 401-412.

13. Brentari, E. G.; and Smith, R. V.: Nucleate and Film Pool Boiling Design Correlations for O_2, N_2, H_2, and He. International Advances in Cryogenic Engineering. Vol. 10. K. D. Timmerhaus, ed., Plenum Press, 1965, pp. 325-341.

14. Larkin, B. K.: Heat Flow to a Confined Fluid in Zero Gravity. Progress in Astronautics and Aeronautics. Vol. 20. G. B. Heller, ed., Academic Press, Inc., 1967, pp. 819-832.

15. Bornhorst, W. J.; and Hatsopoulos, G. N.: Analysis of a Liquid Vapor Phase Change by the Methods of Irreversible Thermodynamics. J. Appl. Mech., vol. 34, no. 4, Dec. 1967, pp. 840-846.

16. Dwyer, Robert F.; Cook, Gerhard A.; and Berwaldt, Oren E.: The Thermal Conductivity of Solid and Liquid Parahydrogen. J. Chem. Eng. Data, vol. 11, no. 3, July 1966, pp. 351-353.

17. Schmidt, A. F.; Purcell, J. R.; Wilson, W. A.; and Smith, R. V.: An Experimental Study Concerning the Pressurization and Stratification of Liquid Hydrogen. Advances in Cryogenic Engineering. Vol. 5. K. D. Timmerhaus, ed., Plenum Press, 1960, pp. 487-504.

18. Roder, Hans M.; and Goodwin, Robert D.: Extended Tables of Provisional Thermodynamic Functions for Para-Hydrogen (British Units); in Liquid, Fluid and Gaseous States at Pressures to 5000 PSI., 36° to 180°R and at Pressures to 1500 PSIA., 140° to 540°R. Rep. 7220, National Bureau of Standards, Jan. 3, 1962.

19. Gebhart, Benjamin: Heat Transfer. McGraw-Hill Book Co., Inc., 1961.

20. Scott, Russell B.: Cryogenic Engineering. D. Van Nostrand Co., Inc., 1959.

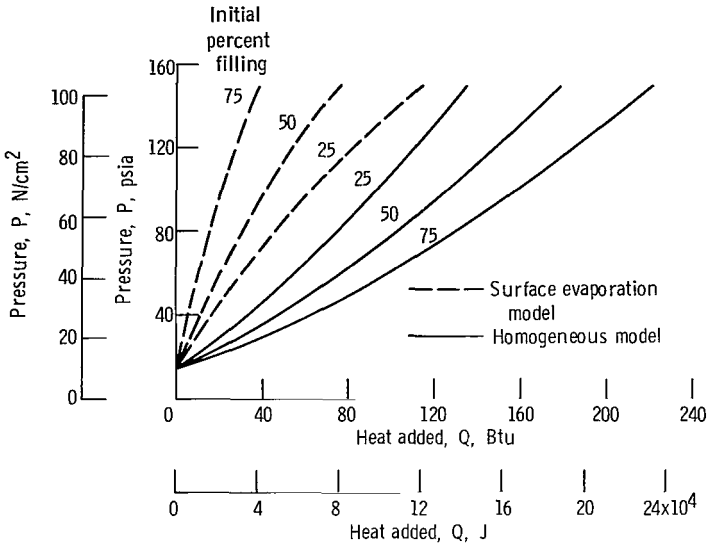

Figure 1. - Tank pressure as function of heat added for two energy distribution models. Tank size, 1 cubic foot (2.832×10^{-2} m^3).

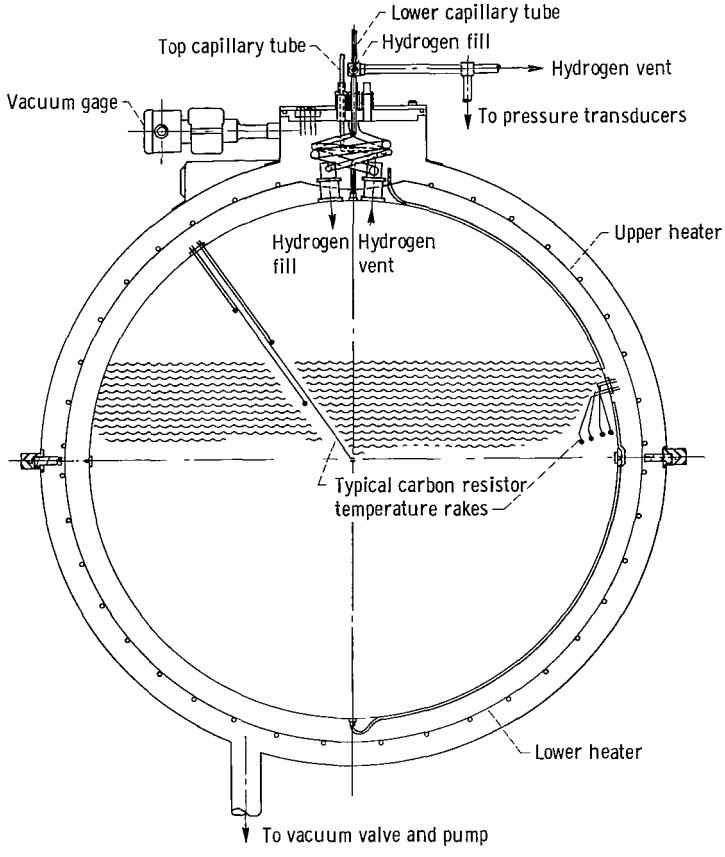

Figure 2. - Liquid-hydrogen experiment apparatus.

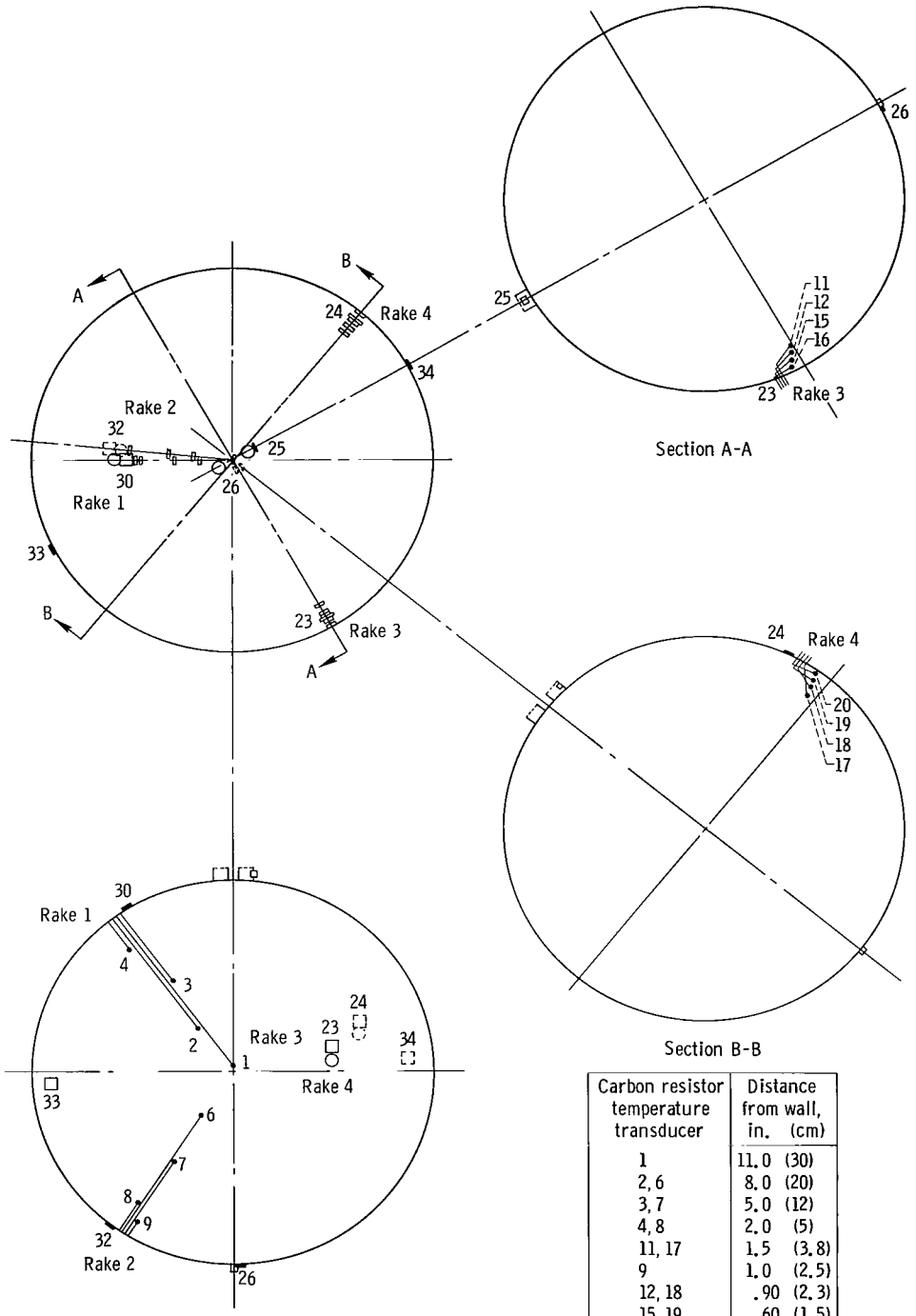

Carbon resistor temperature transducer	Distance from wall, in. (cm)
1	11.0 (30)
2, 6	8.0 (20)
3, 7	5.0 (12)
4, 8	2.0 (5)
11, 17	1.5 (3.8)
9	1.0 (2.5)
12, 18	.90 (2.3)
15, 19	.60 (1.5)
16, 20	.20 (.5)

Figure 3. - Inner-sphere temperature transducer locations. Surface-temperature-transducer 23, 24, 25, 26, 30, 32, 33, and 34 locations shown in drawing.

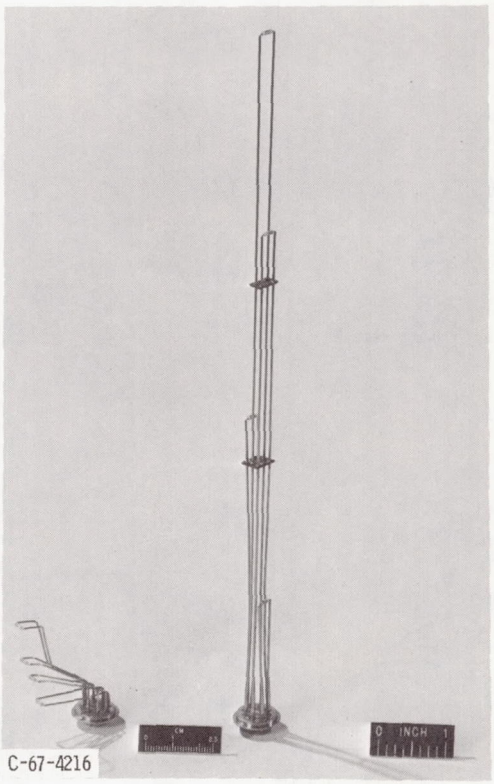

Figure 4. - Carbon resistor rakes.

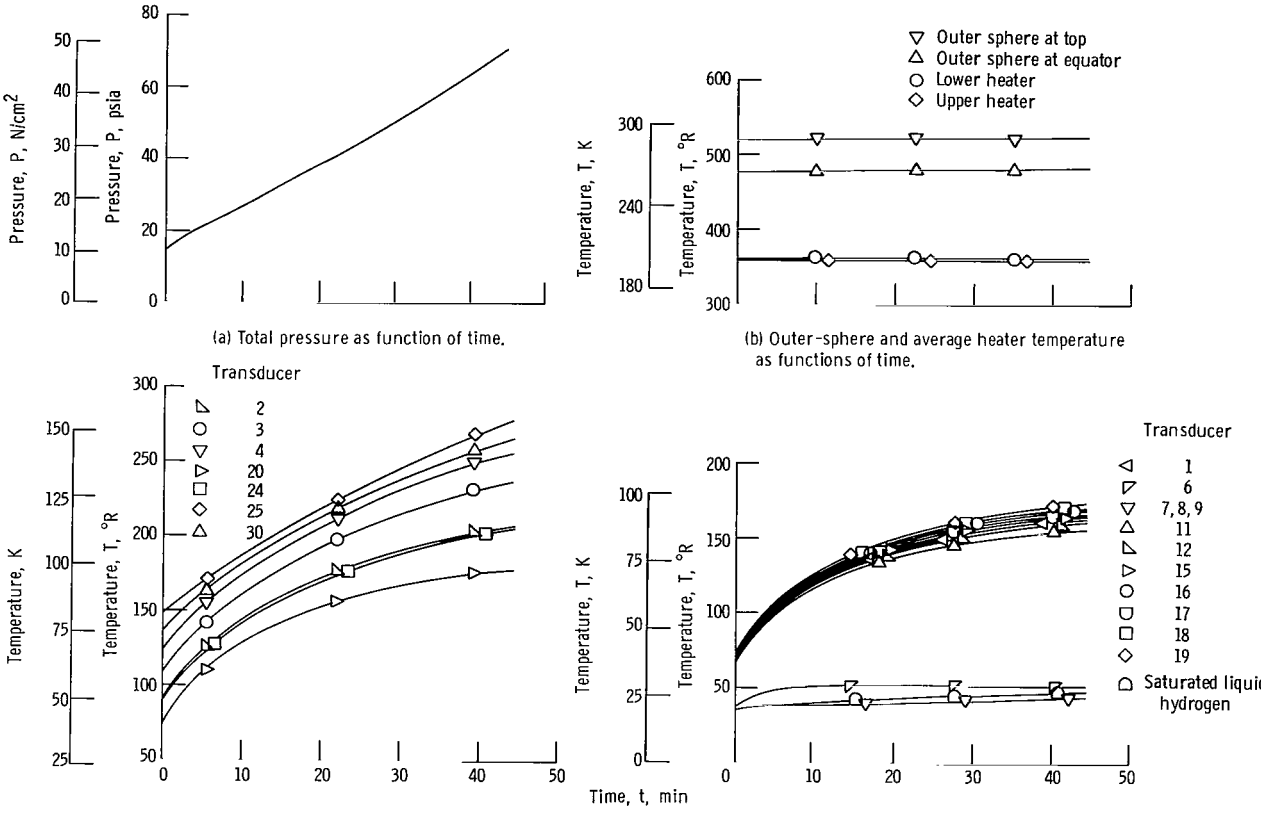

(a) Total pressure as function of time.

(b) Outer-sphere and average heater temperature as functions of time.

(c) Upper inner-sphere internal and surface temperature as functions of time.

(d) Lower inner-sphere internal temperature as function of time.

Figure 5. - Test 1. Initial filling, 31.6 percent; average heat flux, 16.9 Btu per hour per square foot (53 W/m^2). (See fig. 3 for location of transducers.)

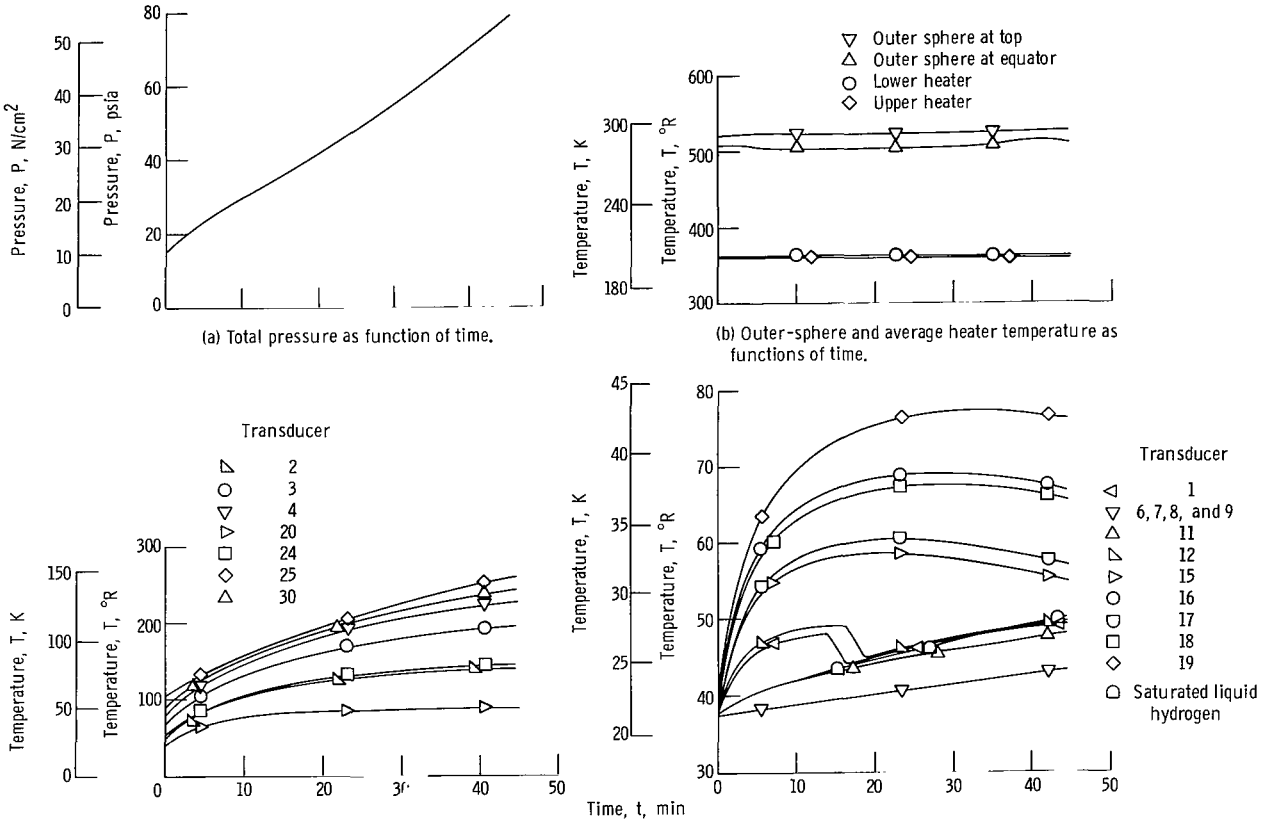

(a) Total pressure as function of time.

(b) Outer-sphere and average heater temperature as functions of time.

(c) Upper inner-sphere internal and surface temperature as functions of time.

(d) Lower inner-sphere internal temperature as function of time.

Figure 6. - Test 2. Initial filling, 48.9 percent; average heat flux, 18.9 Btu per hour per square foot (60 W/m^2). (See fig. 3 for location of transducers.)

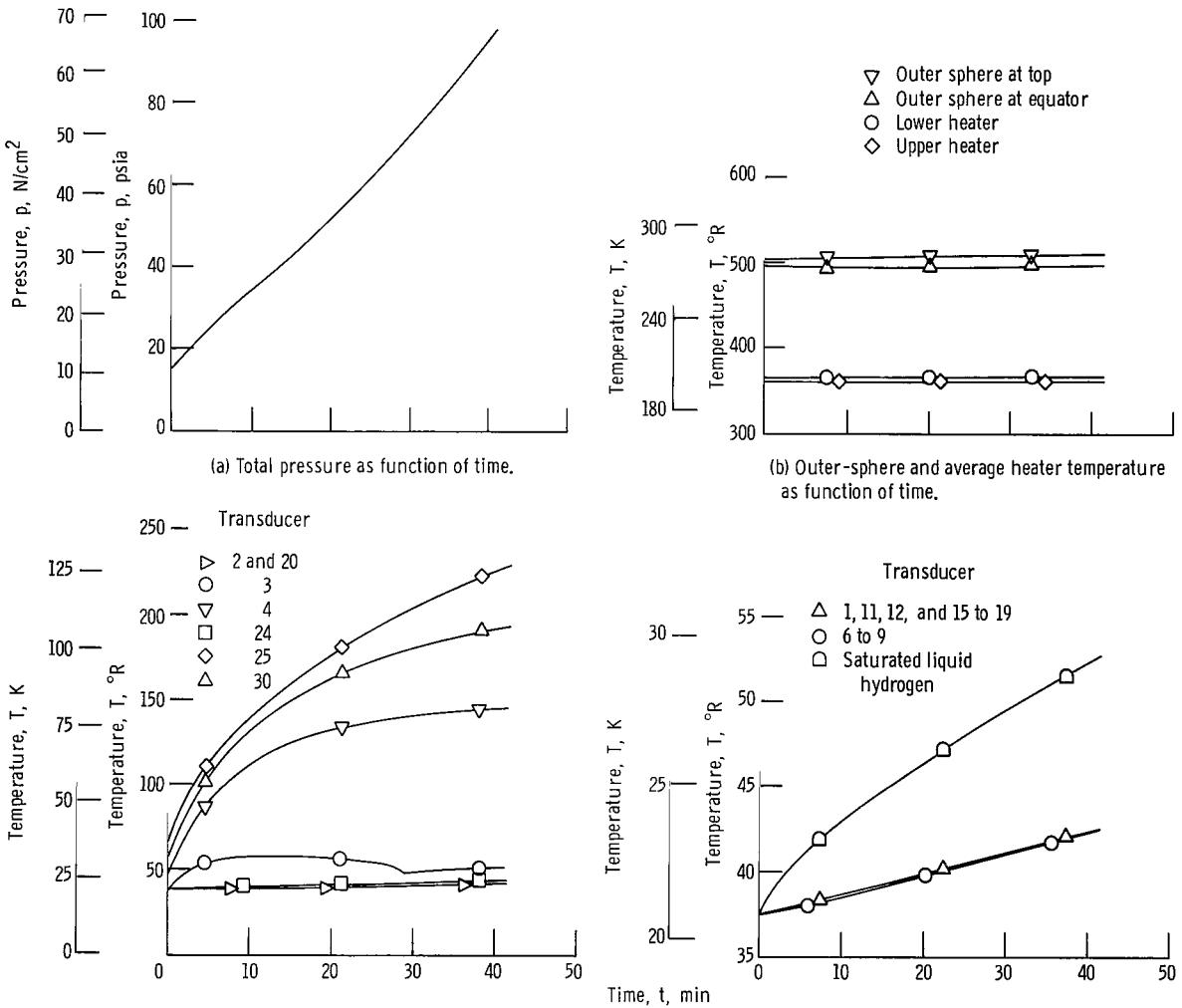

(a) Total pressure as function of time.

(b) Outer-sphere and average heater temperature as function of time.

(c) Upper inner-sphere internal and surface temperature as functions of time.

(d) Lower inner-sphere internal temperature as function of time.

Figure 7. - Test 3. Initial filling, 79.8 percent; average heat flux, 21.9 Btu per hour per square foot (69 W/m^2). (See fig. 3 for location of transducers.)

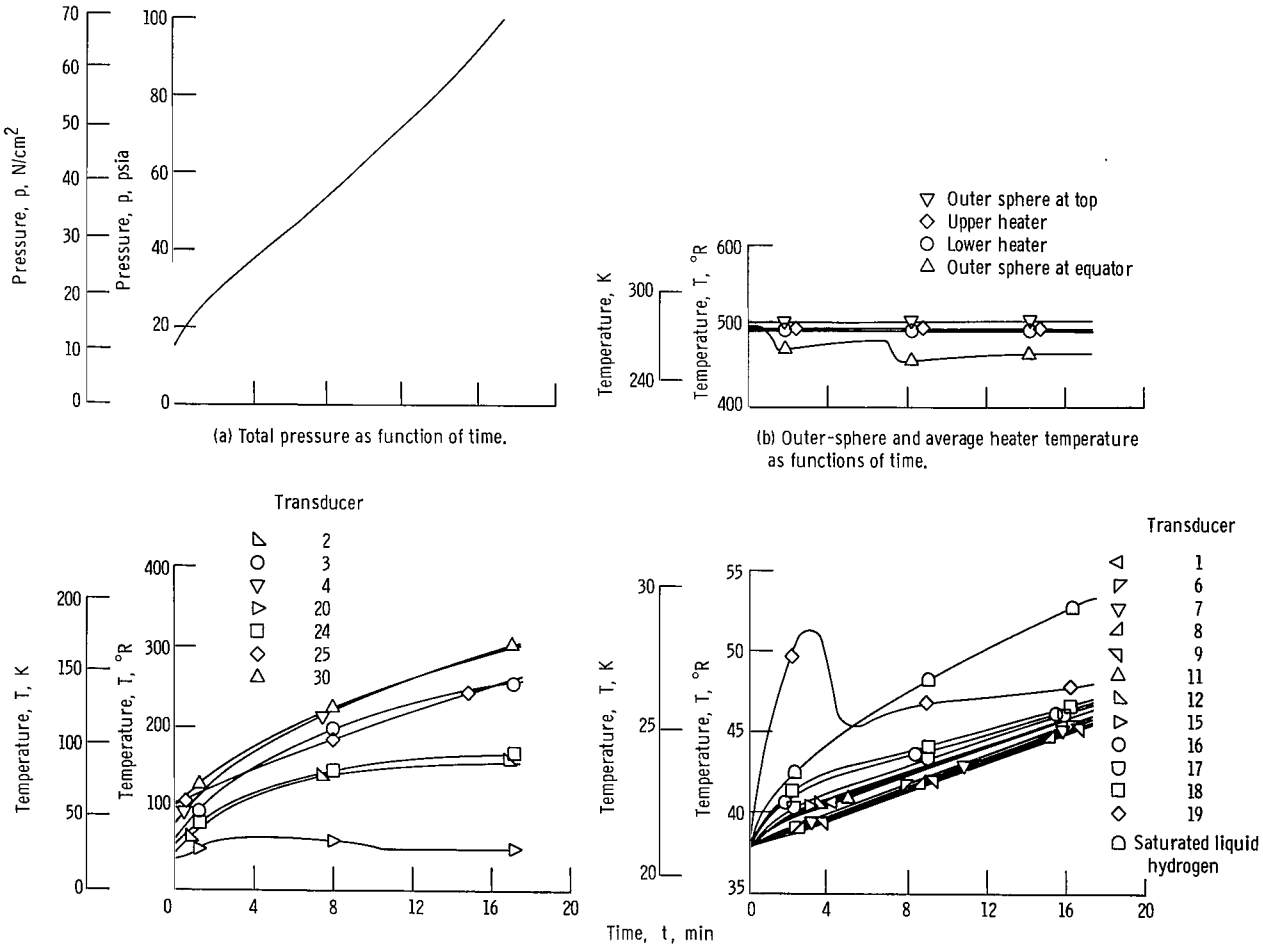

Figure 8. - Test 4. Initial filling, 54.2 percent; average heat flux, 64.4 Btu per hour per square foot (203 W/m^2). (See fig. 3 for location of transducers.)

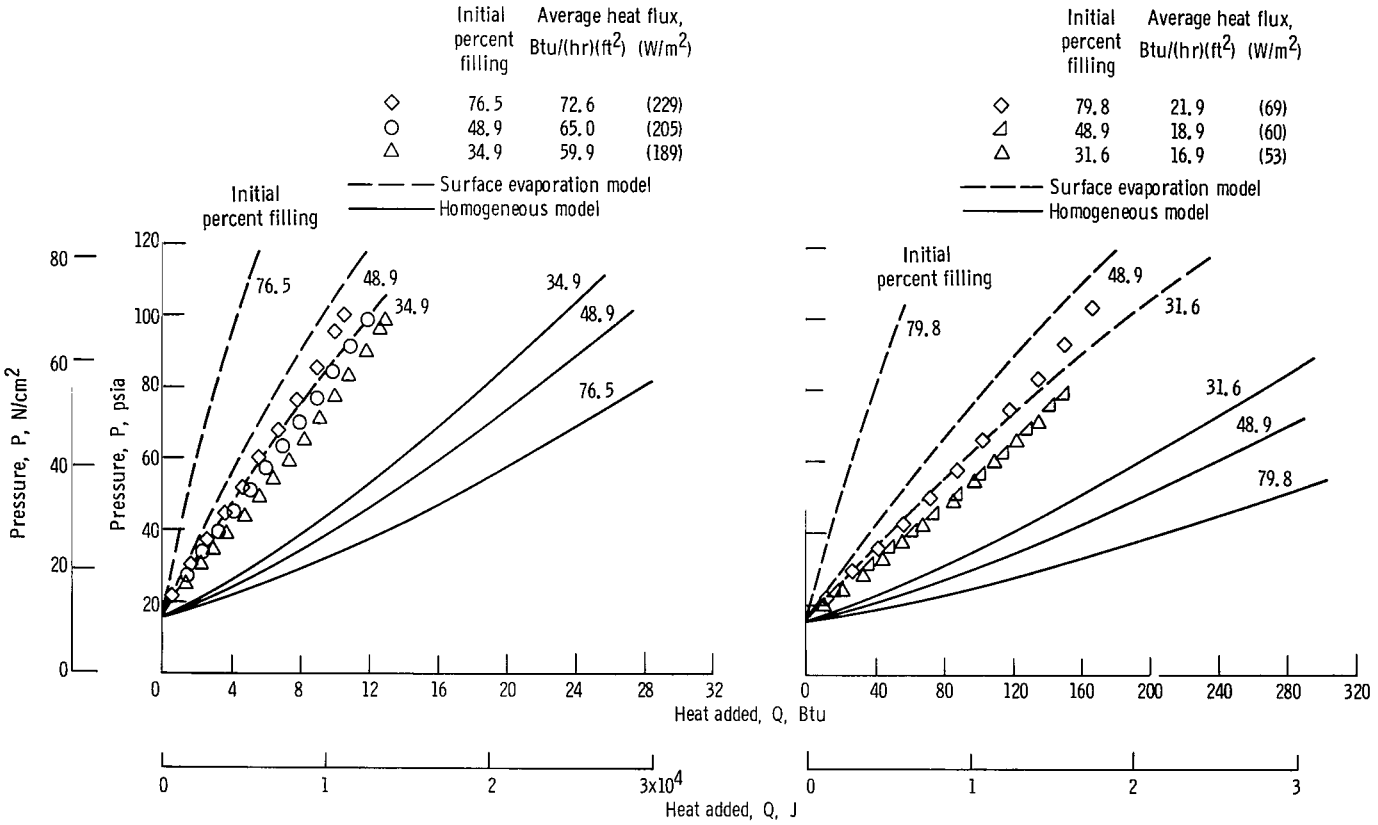

(a) 9-Inch (23-cm) diameter spherical tank (ref. 7).

(b) 22-Inch (56-cm) diameter spherical tank.

Figure 9. - Pressure as function of total heat added, effect of percent filling.

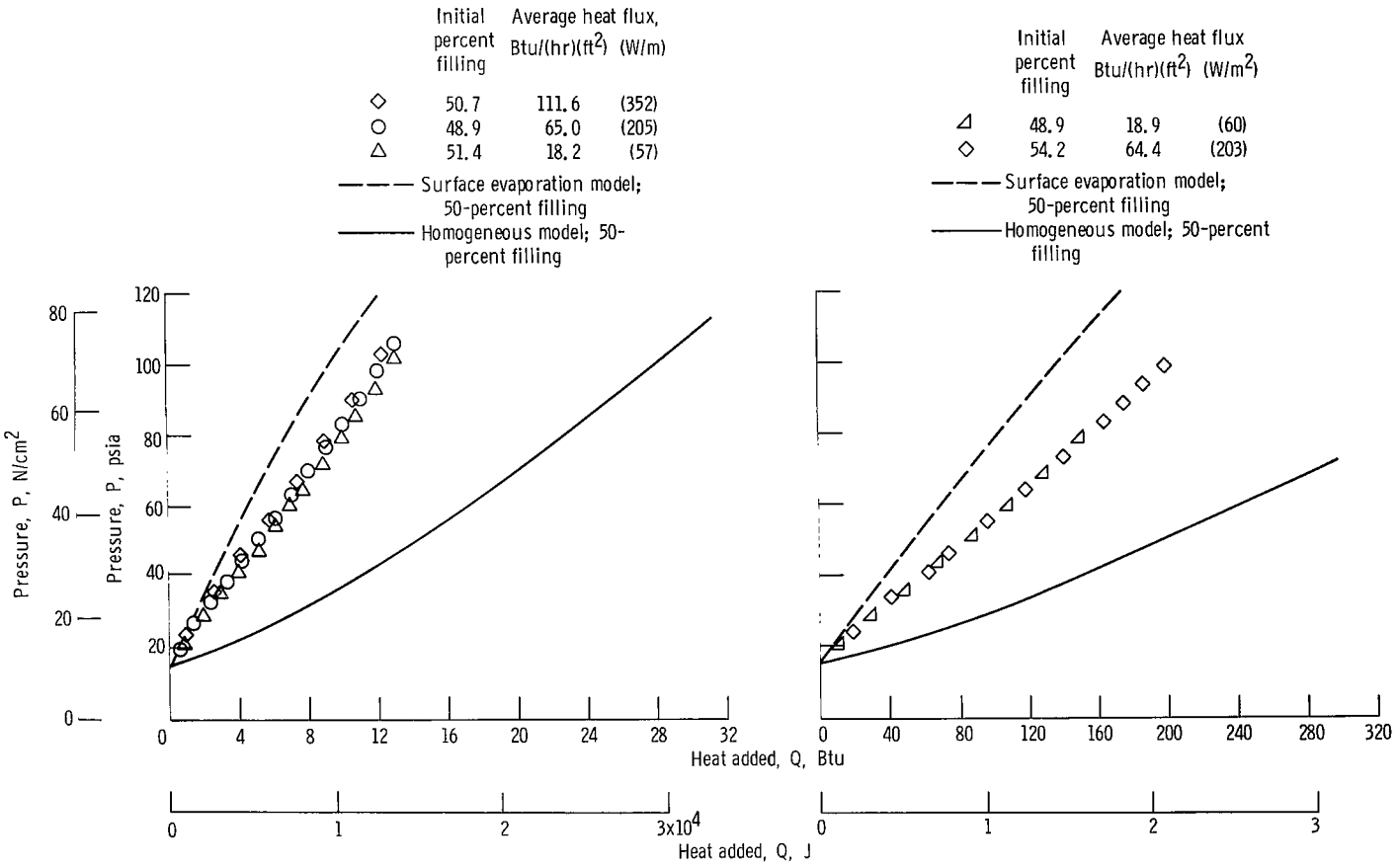

(a) 9-Inch (23-cm) diameter spherical tank (ref. 7).

(b) 22-Inch (56-cm) diameter spherical tank.

Figure 10. - Pressure as function of total heat added; effect of heat-transfer rate.

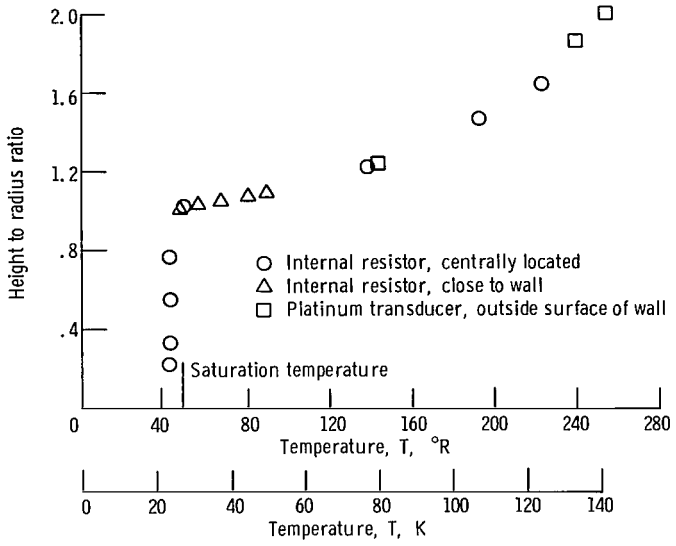

Figure 11. - Inner sphere temperature as function of position for typical 22-inch (56-cm) diameter spherical tank test. Inner-sphere filling, approximately 50 percent.

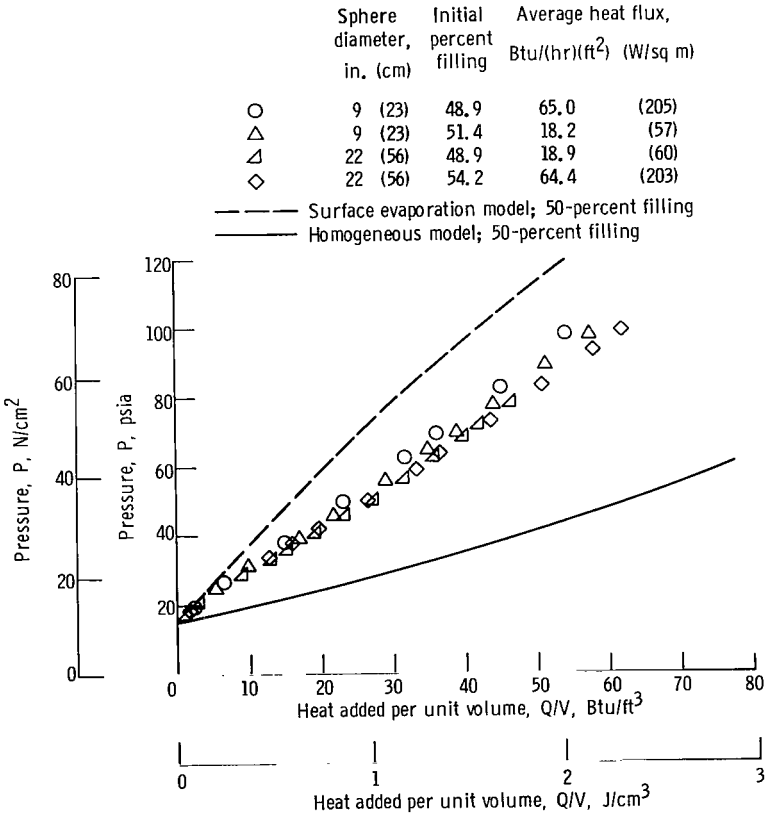

Figure 12. - Pressure as function of total heat added divided by tank volume. (9-in. (23-cm) diam sphere data from ref. 7).

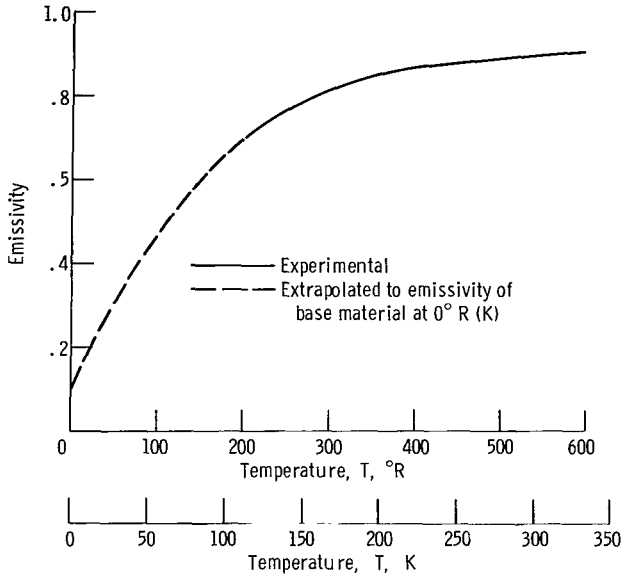

Figure 13. - Inner-sphere and heater emissivity as function of temperature.

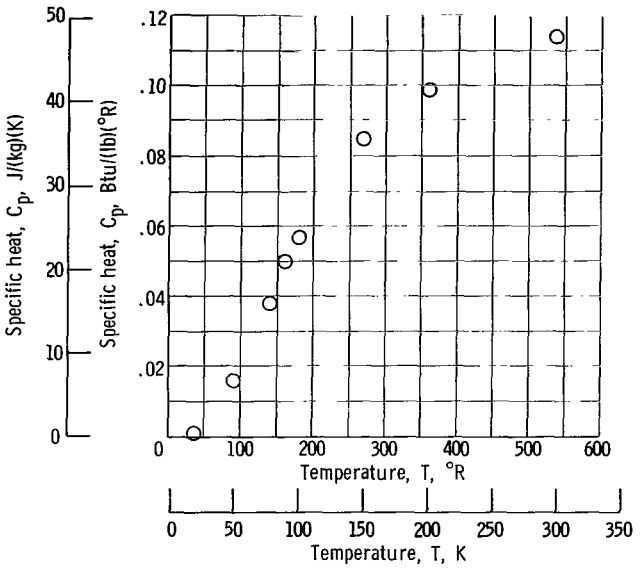

Figure 14. - Stainless-steel specific heat as function of temperature. (Data from ref. 20).

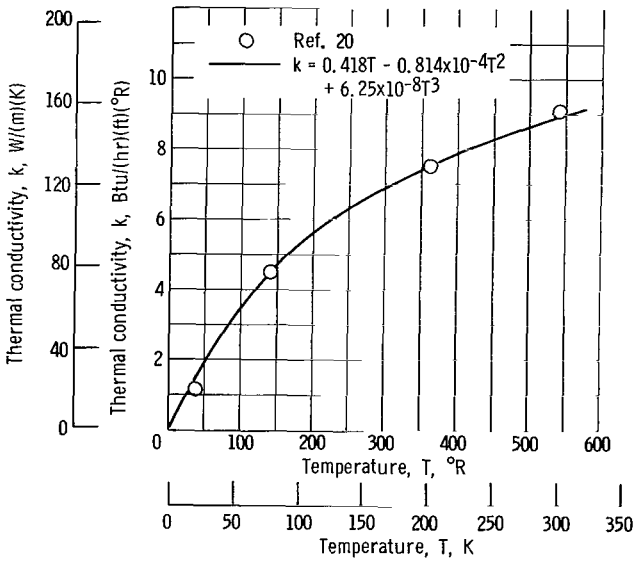

Figure 15. - Stainless-steel thermal conductivity as function of temperature.

NASA-Langley, 1969 —— 33 E-4785

NATIONAL AERONAUTICS AND SPACE ADMINISTRATION
WASHINGTON, D. C. 20546

OFFICIAL BUSINESS

FIRST CLASS MAIL

POSTAGE AND FEES PAID
NATIONAL AERONAUTICS AND
SPACE ADMINISTRATION

"The aeronautical and space activities of the United States shall be conducted so as to contribute . . . to the expansion of human knowledge of phenomena in the atmosphere and space. The Administration shall provide for the widest practicable and appropriate dissemination of information concerning its activities and the results thereof."

—NATIONAL AERONAUTICS AND SPACE ACT OF 1958

NASA SCIENTIFIC AND TECHNICAL PUBLICATIONS

TECHNICAL REPORTS: Scientific and technical information considered important, complete, and a lasting contribution to existing knowledge.

TECHNICAL NOTES: Information less broad in scope but nevertheless of importance as a contribution to existing knowledge.

TECHNICAL MEMORANDUMS: Information receiving limited distribution because of preliminary data, security classification, or other reasons.

CONTRACTOR REPORTS: Scientific and technical information generated under a NASA contract or grant and considered an important contribution to existing knowledge.

TECHNICAL TRANSLATIONS: Information published in a foreign language considered to merit NASA distribution in English.

SPECIAL PUBLICATIONS: Information derived from or of value to NASA activities. Publications include conference proceedings, monographs, data compilations, handbooks, sourcebooks, and special bibliographies.

TECHNOLOGY UTILIZATION PUBLICATIONS: Information on technology used by NASA that may be of particular interest in commercial and other non-aerospace applications. Publications include Tech Briefs, Technology Utilization Reports and Notes, and Technology Surveys.

Details on the availability of these publications may be obtained from:

SCIENTIFIC AND TECHNICAL INFORMATION DIVISION

NATIONAL AERONAUTICS AND SPACE ADMINISTRATION

Washington, D.C. 20546